JACS
JOURNAL OF THE AMERICAN CHEMICAL SOCIETY

Article

pubs.acs.org/JACS

Chiral Plasmonic Films Formed by Gold Nanorods and Cellulose Nanocrystals

Ana Querejeta-Fernández,[†] Grégory Chauve,[‡] Myriam Methot,[‡] Jean Bouchard,[‡] and Eugenia Kumacheva*[,†,⊥,§]

[†]Department of Chemistry, University of Toronto, 80 Saint George Street, Toronto, Ontario M5S 3H6, Canada

[‡]FPInnovations, 570 St. Jean Boulevard, Pointe-Claire, Quebec H9R 3J9, Canada

[⊥]Department of Chemical Engineering and Applied Chemistry, University of Toronto, 200 College Street, Toronto, Ontario M5S 3E5, Canada

[§]The Institute of Biomaterials and Biomedical Engineering, University of Toronto, 4 Taddle Creek Road, Toronto, Ontario M5S 3G9, Canada

Supporting Information

ABSTRACT: Chiral plasmonic films have been prepared by incorporating gold nanorods (NRs) in a macroscopic cholesteric film formed by self-assembled cellulose nanocrystals (CNCs). Composite NR-CNC films revealed strong plasmonic chiroptical activity, dependent on the photonic properties of the CNC host and plasmonic properties of the NRs. The plasmonic chiroptical properties of the composite films were tuned by changing the conditions of film preparation. The strategy presented herein paves the way for the scalable and cost-efficient preparation of plasmonic chiral materials.

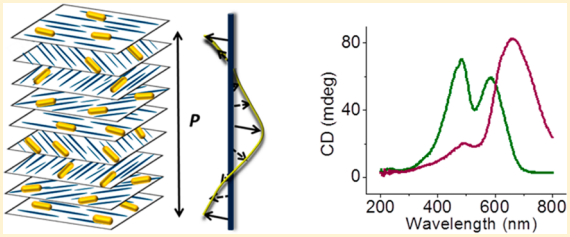

INTRODUCTION

Chiral plasmonic nanostructures offer the ability to achieve strong optical circular dichroism (CD) activity over a broad spectral range,[1,2] which has been challenging for chiral molecules. Materials derived from such nanostructures are expected to enrich the field of metamaterials with negative refraction,[3−5] nonlinear optics,[6] and nanolevitation[7] properties. Promising applications of chiral plasmonic nanostructures also include circular polarizers,[8] detectors for circularly polarized light,[9] asymmetric catalysts,[10] and sensors of biomolecules.[11,12]

Both fundamental studies and applied research in the field of chiral plasmonic materials critically depend on the availability of reliable and robust methods of their preparation. Currently, plasmonic chiroptical systems can be classified into three groups: (i) individual nanoparticles (NPs) with chiral geometry[13] and achiral NPs capped with chiral ligands,[14] (ii) discrete chiral assemblies of achiral NPs[15−23] and assemblies of chiral NPs,[24,25] and (iii) macroscopic mixtures of achiral NPs with chiral nematic liquid crystals.[26−30] The last system has been used to induce chiral organization of close-to-spherical plasmonic NPs[31] and nanorods (NRs),[30] yet plasmonic chiroptical activity of NPs within cholesteric liquid crystals has not been reported. Furthermore, the utilization of solid nanostructured cholesteric hosts, whose helical structure can be tuned in its own right, remains elusive.

In particular, in comparison with shape-isotropic metal NPs,[32,33] the utilization of plasmonic NRs offers superior chiroptical activity,[18a] which is represented by strong CD and polarization rotator characteristics. In addition, the ability to vary the aspect ratio of gold NRs provides a useful strategy for fine-tuning of their chiroptical plasmonic properties.

Herein we present a new composite chiroptical plasmonic material and a straightforward, cost-efficient strategy for its fabrication. The approach utilizes the incorporation of guest gold NRs into a macroscopic cholesteric solid film formed by cellulose nanocrystals (CNCs). It is currently well-established that in relatively concentrated suspensions whisker-like CNCs spontaneously phase separate to form an isotropic and a cholesteric liquid crystalline phases.[34] The chiral nematic order of the latter is largely preserved in dry films,[35] in which adjacent CNC layers rotate anticlockwise with respect to each other and form a left-handed helical structure.[34,36−38] The CNC films exhibit the properties of a chiral photonic crystal with a strong circular dichrosim.[35] Importantly, the position of the stop band for the CNC film can be tuned from the visible to the near-infrared spectral range by changing the conditions of film preparation, e.g., by ultrasonication or by adding electrolytes to the CNC suspension.[36,37,39,37,40] A cholesteric liquid crystalline phase formed by CNCs has been used as a template to synthesize chiral mesoporous silica[41] and carbon,[42] which were subsequently decorated with metal NPs;[43,44] however, a direct use of CNC films as a host for the organization of metal NPs, and especially, of plasmonic NRs has not been reported.

The method and the material reported in the present work offer the following new and potentially useful features: (i) the

Received: February 27, 2014
Published: March 3, 2014

   dx.doi.org/10.1021/ja501642p | J. Am. Chem. Soc. 2014, 136, 4788−4793

chiroptical activity of plasmonic NRs that is significantly stronger than that measured for discrete chiral objects in solutions; (ii) parallel orientation of the long axes of CNCs and NRs, both perpendicular to the direction of the left-handed helix, thereby yielding a new type of plasmonic chiral pattern; (iii) a synergy between the structure and optical properties of the photonic CNC host and plasmonic NRs; (iv) the tunability of circular dichrosim of the hybrid film; (v) the robust, free-standing nature of the composite film; and (vi) the simplicity of film preparation, as well as the abundance and renewable character of CNCs.

EXPERIMENTAL SECTION

An aqueous suspension of CNCs with the length and average diameter of 100−200 and ∼17 nm, respectively, was obtained from FPInnovations (Canada). Gold NRs with an average length and diameter of 41 and 14 nm, respectively, were synthesized by the seed-growth method.[45] These dimensions of the NRs and CNCs were selected to avoid the spectral overlap of the longitudinal extinction band of the NRs and the stop band of the CNC film. Furthermore, the similarity in diameters of CNCs and NRs was expected to favor the integration of NRs within the planar CNC layers and preserve the chiral self-assembly of CNCs.

Two aqueous suspensions, one comprising gold NRs and the other one CNCs, were mixed in varying CNC-to-NR weight ratios. The mixed suspension was poured into a Petri dish as a 4-mm-thick liquid layer. The water was evaporated for 2 days under ambient conditions, thereby mimicking the conditions of the preparation of NR-free chiral CNC films.[35]

RESULTS AND DISCUSSION

Figure 1 illustrates the approach to the preparation of chiral composite plasmonic films, which is based on the co-assembly

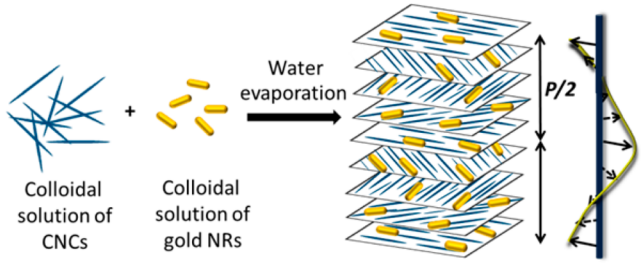

Figure 1. Schematic of the preparation of the composite chiroptical plasmonic film by mixing aqueous suspensions of CNCs and gold NRs. Upon slow evaporation of water, the CNCs form a left-handed liquid crystalline cholesteric phase and, eventually, NR-loaded solid film. Arrows show the average direction of orientation of the CNCs (director) in the film. The twist of the director in the adjacent CNC layers generates a helix along the direction perpendicular to the layers. *P* is the helical pitch or the distance over which the director undergoes a full 360° twist.

of CNCs and gold NRs. We hypothesized that the opposite electrostatic charges of the anionic CNCs (carrying surface sulfonic acid ester groups) and cationic NRs (stabilized with cetyltrimethylammonium bromide (CTAB)) would favor attraction between these species in the mixed suspension and will lead to the chiral assembly of the NRs in the host cholesteric films.

Figure 2a,b shows representative transmission electron microscopy (TEM) images of the CNCs and gold NRs, respectively. The electrokinetic potentials (ζ-potentials) of the

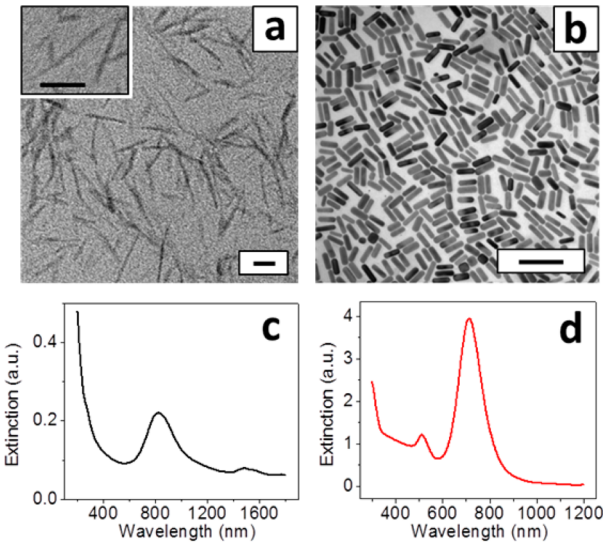

Figure 2. Representative TEM images of (a) CNCs and (b) gold NRs. Inset in (a) shows high magnification of the CNCs. Extinction spectra of the (c) CNC film dry-cast from a 2.44 wt% CNC suspension and (d) of the suspension of gold NRs at NR concentration of 1.01 nM. Scale bars are 100 nm.

as-prepared NRs and CNCs were +27 and −47 mV, respectively.

Figure 2c shows the extinction spectrum of the NR-free CNC film. The spectrum shows a broad stop band in the 630−1200 nm spectral range, with the maximum centered at 830 nm, and two peaks in the IR spectral range, corresponding to glucose molecules.[46] The stop band corresponds to the wavelength, λ_{sb}, reflected by the CNC film, due to the periodicity in the orientation of the CNCs. We estimated the cholesteric pitch *P*, the distance over which the helix undergoes a complete turn (Figure 1). The spectral position of the stop band is

$$\lambda_{sb} = nP \sin\theta \quad (1)$$

where *n* is the effective refractive index of the CNC film, and θ is the angle of incidence of light.[47] For λ_{sb} = 830 nm, n = 1.54,[48] and θ = 90°, the value of *P* for the CNC film was calculated to be 539 nm. Increase in extinction of the CNC film at λ < 400 nm originated from absorption of light at the molecular level.[49]

The extinction spectrum of gold NRs exhibited characteristic transverse and longitudinal localized surface plasmon resonances (TLSPR and LLSPR, respectively) at 512 and 714 nm, respectively (Figure 2d).

We prepared composite NR-CNC films by mixing 5 mL of 2.44 wt% CNC suspension with 1 mL of the suspension of gold NRs at a particular concentration of NRs. The estimated NR concentration in the composite films, C_{NR}, varied from 0.12 to 3.39 wt% (Table S1, SI). As a control system we used a NR-free CNC film prepared by adding 1 mL of water to the CNC suspension. The composite films had an average thickness of ∼30 μm and exhibited iridescence characteristic for the photonic crystal structure.[50,51] A dark-red color of the films originated from the extinction of gold NRs (Figure S2, SI).

Figure 3a−c shows representative SEM images of the cross-section of the films, which revealed the periodicity of the chiral nematic structure in the direction perpendicular to the CNC layers. The periodic spacing corresponded to the layers with similar CNC orientation, that is, to *P*/2 (see Figure 1).[52,53] The

dx.doi.org/10.1021/ja501642p | J. Am. Chem. Soc. 2014, 136, 4788−4793

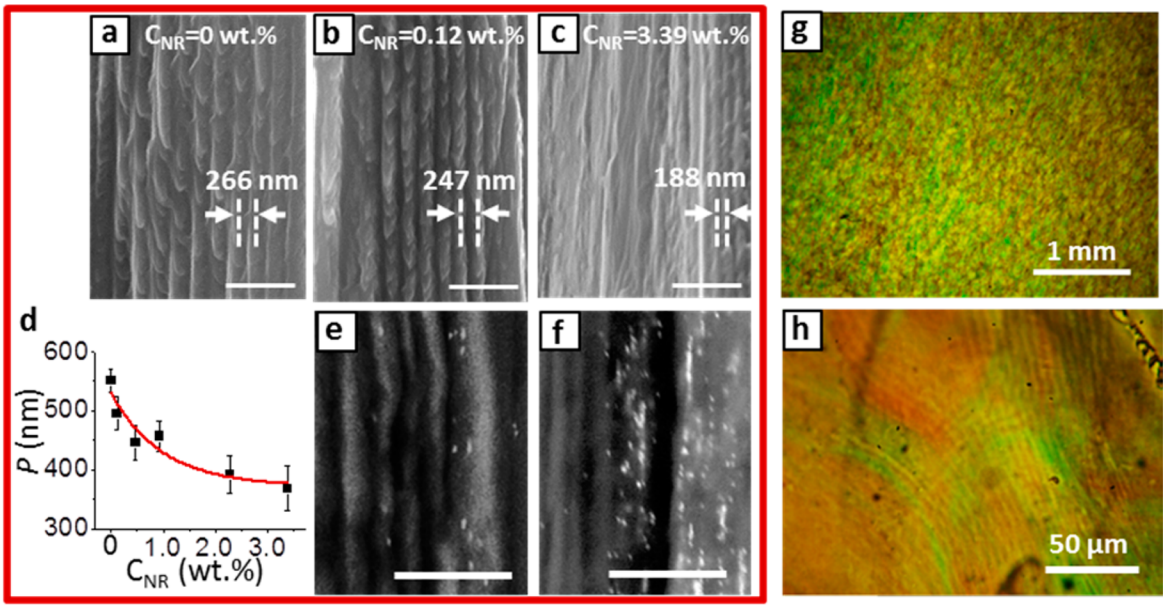

Figure 3. (a–c) Representative SEM images of the cross-section of the NR-CNC films at NR concentrations of (a) 0, (b) 0.12 wt% (the lowest NR concentration), and (c) 3.39 wt% (the highest NR concentration). The periodicity corresponding to $P/2$ is indicated on the images. (d) Variation of the average pitch, plotted as a function of NR content in the composite films. The red line represents an exponential fit of the data. Each point was obtained as the average of at least 15 measurements performed along the direction perpendicular to the periodic structure in at least, 3 different images. (e,f) Representative SEM images of the cross-section of the composite films acquired with the backscattered electron detector. Gold NRs appear as bright spots. (Scale bars in a–c, e, and f are 1 μm.) (g) Low- and (h) high-magnification polarization microscopy images of the NR-CNC film at C_{NR} = 0.47 wt%.

helical pitch of the NR-free CNC film (Figure 3a) was 551 nm, in agreement with the value of 539 nm determined from the position of the stop-band of this film. For NR content not exceeding 0.93 wt%, the entire composite film had a chiral nematic structure, while at higher NR concentrations, chiral nematic regions constituted only a fraction of the film. Figure 3b,c shows representative cross-sectional SEM images of the composite films with NR content of 0.12 and 3.39 wt%, corresponding to the lowest and highest NR concentration, respectively. In Figure 3c only a small fraction of the film exhibited a chiral nematic structure (shown as a narrow domain on the right side of the image). Progressive disappearance of the chiral nematic structure with increasing NR content was strongly affected by the increasing content of NRs and in particular, CTAB introduced in the system with the NRs (Figure S4, SI).

The increase in NR content in the film also resulted in the decrease of pitch P of the chiral nematic structure (Figure 3a–d). Figure 3d shows that with NR concentration increasing from 0 to 3.39 wt%, the value of P reduced from 551 to 368 nm, respectively. Such a decrease in P could be ascribed to the reduction of the distance between the layers of negatively charged CNCs due to the presence of cationic species (both CTAB-coated NRs and free CTAB molecules) bridging the CNCs.[36]

Figure 3e,f shows the cross-sectional SEM images acquired with a backscattered-electron detector. Gold NRs appear bright on the background of the dark CNC host, due to their higher electron density than the organic matrix. The NRs were localized in "parallel lines" characteristic of the organization of the CNCs layers, with a fraction of them localized in the achiral nematic domains, which suggested a similar alignment of the NRs and CNCs in the hybrid material. Polarized optical microscopy experiments confirmed the chiral nematic nature of the composite NR-CNC films, at both low and high magnification, as evidenced by the typical texture[41,52,54] (Figure 3g,h, respectively).

The extinction and CD (chiral extinction) properties of the composite films with a different content of NRs, C_{NR}, are shown in Figure 4, along with the properties of NR-free CNC

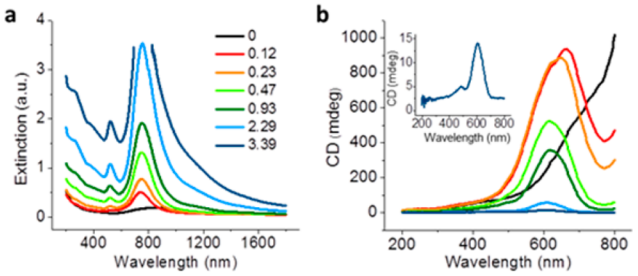

Figure 4. Variation in (a) extinction and (b) CD of the NR-CNC films. The legend indicates NR concentration in the films in wt%. Inset in (b) shows zoomed-in CD spectrum of film at NR content of 3.39 wt %.

films given for comparison. The extinction spectra of the NR-CNC films exhibited two strong peaks at ~750 and ~520 nm, corresponding to the LLSPR and TLSPR peaks of the NRs, respectively (Figure 4a). Both plasmonic bands were red-shifted in comparison with those measured in an aqueous solution (Figure 2d), due to the change in dielectric properties of the surrounding medium.[55] The NR-free CNC film showed a stop band at the same spectral position of ~830 nm as the CNC film dry cast from 2.44 wt% suspension (Figure 2c). No significant change in the spectral position of the NR plasmonic bands occurred with an increasing NR content in the films, indicating both the absence of NR aggregation in the CNC matrix and a

dx.doi.org/10.1021/ja501642p | J. Am. Chem. Soc. 2014, 136, 4788–4793

negligible change of the effective index of refraction of the composite films (Table S3, SI). The intensity of the bands increased with increasing NR content in the films.

Figure 4b shows the CD spectra of the composite films, along with the spectrum of the NR-free CNC film. The latter exhibited a positive CD peak typical of a left-handed chiral nature.[35] The spectra of the NR-CNC films exhibited a strong positive CD signal, which we ascribed to a combined peak corresponding to the chiral CNC matrix and a plasmonic LLSPR mode. This combined CD peak was blue-shifted in comparison with that of the NR-free CNC film. Furthermore, with increasing C_{NR}, the combined CD peak in Figure 4 exhibited blue-shift, in agreement with a decreasing pitch of hybrid films at higher C_{NR} (Figure 3a–d, Table S4, SI). The decrease of the intensity of the CD signal was ascribed to the lower fraction of the regions with a chiral nematic structure in films with a higher C_{NR}. Importantly, we observed the chiral TLSPR peak for the films with C_{NR} varying from 0.93 to 3.39 wt% (inset in Figure 4b and Figure S7, SI). We note that blue-shift of the CD peaks, in comparison with the corresponding extinction peaks, was observed for TLSPR (490 vs 523 nm for C_{NR} = 3.39 wt%) (Table S7, SI), thereby signifying a combined nature of chiroptical activity of hybrid films. We stress that no blue shift occurred in extinction spectra of the composite films with increasing C_{NR} (Figure 4a), which further supported a combined nature of the photonic–plasmonic CD signal, in comparison with plasmonic peaks in extinction spectra. A higher sensitivity of the plasmonic CD signals to changes in the surrounding matrix detected in our work was in agreement with previous observations.[43]

The composite NR-CNC films exhibited a strong dependence of CD on the light incident angle (Figure S12, SI), further underlying the effect of the structure of photonic CNC films on their plasmonic chirality.

In the next step, we showed the capability to tune the induced plasmonic chiroptical activity of the composite films in a two-fold manner: (i) by changing NR dimensions and (ii) by changing the helical pitch of the CNC matrix. We used NRs with the average length and diameters 47 × 20 (Series A), 33 × 11 (Series B), and 36 × 9 nm (Series C). Figure 5 shows the effect of NR dimensions on extinction and CD properties of the composite films, with the corresponding TEM images of the NRs shown in insets. Figure 5a–c (dashed lines) shows characteristic TLSPR and LLSPR bands of the NRs in the colloidal solutions. With the NR aspect ratio increasing from 2.4 to 3.0 and then to 4.0 (Series A, B, and C, respectively), the plasmonic bands red-shifted. In the composite films, further red-shift was observed due to the change of dielectric properties of the surrounding medium (Figure 5a–c, solid lines).

Figure 5d–f shows the variation in CD spectra of the corresponding composite films. A single peak was the result of combined CD signal of the CNC matrix and the LLSPR mode of the NRs (the TLSPR modes were distinguishable at high C_{NR} (Figure S8, SI). The variation in CD signal of the composite films correlated with the red-shift in extinction of the NRs in the A-B-C series. Importantly, composite NR-CNC films prepared with the NRs of Series B and C (the NR diameter of 10 ± 1 nm) had a similar pitch of 440 and 447 nm (Table S5, SI). Yet, the CD signal in Figure 5e,d featured a ~23 nm red-shift, consistent with the increase in NR aspect ratio. This effect further supported NR contribution to the chiroptical activity of the composite films. Furthermore, films prepared at relatvely high C_{NR} clearly revealed both the TLSPR and LLSPR

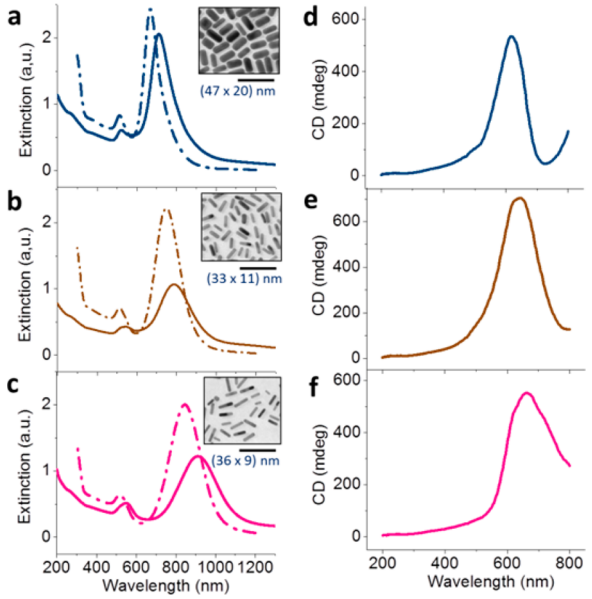

Figure 5. Tuning chiroptical activity of NR-CNC composite films by varying NRs dimensions. (a–c) Extinction (solid lines) and (d–f) corresponding CD spectra of the composite films prepared from NRs of different sizes. Insets in (a–c) show TEM images of the NRs and their sizes. (Scale bars in insets are 100 nm). C_{NR} = 0.47 wt%. Dashed spectra in (a–c) correspond to the colloidal solutions of gold NRs.

plasmonic CD modes, whose spectral position correlated with the aspect ratio of the NRs of B and C series (Figure S8, Table S10, SI).

The CD spectra in Figure 5 exhibited blue-shift, in comparison with the corresponding extinction spectra. We also note that even films loaded with 20 nm-diameter NRs, whose diameter was larger than that of the CNCs, showed strong chiroptical activity.

Next, we tuned the chiral plasmonic properties of the composite films by varying the helical pitch P of the CNC matrix, while maintaining NR dimensions and concentration constant. Prior to film casting, a varying amount of electrolyte (NaCl) was added to the mixed NR-CNC suspensions. We first examined the effect of NaCl concentration, C_{NaCl}, on the extinction spectra of the NR-free CNC films (Figure 6a and Figure S9, SI). The spectral position of the stop band (Bragg reflection), λ_{sb}, of the CNC films blue-shifted with increasing C_{NaCl}, indicating the reduction of the helical pitch of the CNC films (eq 1). This effect has been previously reported for chiral nematic CNC suspensions and attributed to the reduction in electrostatic repulsion between the CNCs in the presence of salts.[39,40] At C_{NaCl} = 2.13 wt% the stop band associated with the helical structure of the film disappeared (Figure 6a, violet spectrum, and Figure S10, SI). The variation in CD spectra of the CNC films (Figure 6b) correlated with the change in their extinction properties, including the disappearance of chiroptical activity in films with the highest NaCl concentration of 2.13 wt % (Figure 6b, violet spectrum). These films lacked the chiral nematic structure, which was confirmed by their SEM imaging (Figure S5, SI).

The composite films with a varying C_{NaCl} exhibited the characteristic plasmonic peaks (Figure 6c). For C_{NaCl} < 0.13 wt % the LLSPR peak overlapped with the stop band of the CNC host. For C_{NaCl} of 0.13 and 0.22 wt% the signature of the stop band appeared on the right and left side of the TLSPR peak,

dx.doi.org/10.1021/ja501642p | J. Am. Chem. Soc. 2014, 136, 4788–4793

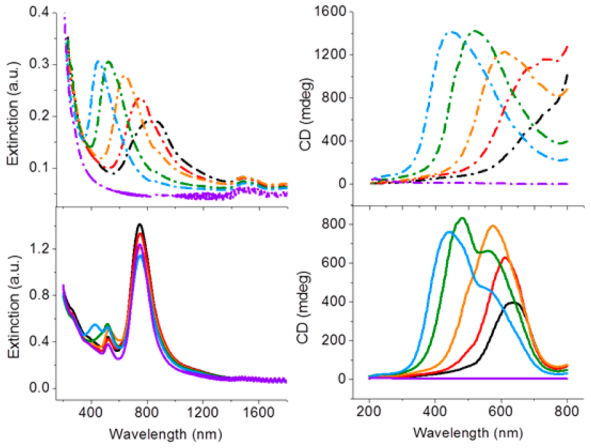

Figure 6. Tuning chiroptical activity of the NR-CNC composite films by adding NaCl to the mixed NR-CNC suspensions. (a) Extinction and (b) CD spectra of the NR-free CNC films (dashed lines), and (c) extinction and (d) CD spectra of the NR-CNC films (solid lines) at NaCl of 0 (black color), 0.02 (red color), 0.06 (orange color), 0.13 (green color), 0.22 (blue color), and 2.13 (violet color) wt%. In (c) and (d), C_{NR} = 0.47 wt.%.

respectively, and at C_{NaCl} = 2.13 wt% stop band disappeared, similarly to the NR-free CNC films.

Figure 6d shows the CD spectra of the NR-CNC films prepared at varying C_{NaCl}. We identified two spectral regions according to the position of λ_{sb} relative to the LLSPR of the NRs, namely, $\lambda_{sb} \approx \lambda_{LLSPR}$ ($0 \leq C_{NaCl} \leq 0.02$ wt%) and $\lambda_{sb} < \lambda_{LLSPR}$ ($0.06 \leq C_{NaCl} \leq 0.22$ wt%). The TLSPR mode was not discernible in Figure 6d. In the first region, spectral overlap of the chiroptical activity of the CNC matrix and the NRs led to a single strong CD peak (Figure 6d, black and red spectra), similar to the results shown in Figure 4b. With increasing C_{NaCl} the change in the structure of the CNC matrix led to the blue-shift of the CD peak, as shown in Figure 6b. As a result, a new peak corresponding to the CNC host emerged in the CD spectra of the composite films, first, as a shoulder at ~500 nm (Figure 6d, orange spectrum) and then as a distinct second peak coexisting with a NR CD peak (Figure 6d, green and blue spectra, 565 and 559 nm, Figure S11 and Table S11, SI). Thus for $0.06 \leq C_{NaCl} \leq 0.22$ wt% the CD spectra of the composite films exhibited two signals: one associated with the CNC host and the other one with plasmonic chiroptical activity of the NRs. Importantly, both CD peaks disappeared at high salt concentration of 2.13 wt% (Figure S10, SI), indicating the critical role of the long-range chiral periodic order on the induced plasmonic chiroptical activity of the NRs.

At the moment, we cannot explain increase in CD intensity with increasing salt concentration, however the variation in CD intensity was similar for the composite and NR-free films.

The results shown in Figures 4–6 demonstrate the ability to tune the spectral range and intensity of plasmonic chiroptical activity of the composite NR-CNC films by changing NR concentration, NR dimensions and by adding a salt to the NR-CNC suspensions. Other methods such as the change in CNC dimensions and surface chemistry, the variation in preparation procedures of the NR-CNC films and the application of external fields[39,37] can be used to explore a synergetic influence of NRs and CNCs on plasmonic chiroptical activity of the composite films.

CONCLUSION

In summary, we have shown the generation of composite NR-CNC films with strong plasmonic chiroptical activity. The interesting properties of the films originate from the interaction of the photonic properties of the CNC matrix (caused by its long-range cholesteric order) and plasmonic properties of gold NRs. The composite chiral plasmonic material exhibited tunable chiroptical characteristics, which are beneficial for fundamental studies of collective plasmonic chiroptical activity properties and their potential applications. The ease and robustness of film preparation make the method and the composite material particularly attractive. Further studies such as theoretical analysis are needed to gain insight in the mechanism of plasmonic CD activity and possible interference effects in this novel type of metamaterial.

ASSOCIATED CONTENT

Supporting Information

Materials, description of methods, effect of CTAB and NaCl content on the stop band of CNC films, SEM images, and CD spectra of the CNC films and composite NR-CNC films. This material is available free of charge via the Internet at http://pubs.acs.org.

AUTHOR INFORMATION

Corresponding Author

ekumache@chem.utoronto.ca

Notes

The authors declare no competing financial interest.

ACKNOWLEDGMENTS

The authors thank Engage Grant (NSERC Canada) for financial support of this work. The authors are grateful to FPInnovations for providing the samples of CNCs. The authors thank Prof. Ron Kluger for the use of CD spectropolarimeter and Prof. Derek Gray for discussion of experimental results. The authors thank Prof. Kun Liu for assistance in NR synthesis. The authors thank Dr. Ilya Gourevich and Dr. Neil Coombs (Centre for Nanostructure Imaging at Department of Chemistry, University of Toronto) for valuable assistance in acquisition of SEM images. The authors thank Ilya Gourevich, Dr. Neil Coombs, and the Centre for Nanostructured Imaging at Department of Chemistry, University of Toronto.

REFERENCES

(1) Guerrero-Martínez, A.; Alonso-Gómez, J. L.; Auguié, B.; Cid, M. M.; Liz-Marzán, L. M. *Nano Today* **2011**, *6*, 381–400.
(2) Valev, V. K.; Baumberg, J. J.; Sibilia, C.; Verbiest, T. *Adv. Mater.* **2013**, *25*, 2517–2534.
(3) Tretyakov, S.; Nefedov, I.; Sihvola, A.; Maslovski, S.; Simovski, C. *J. Electromagn. Waves Appl.* **2003**, *17*, 695–706.
(4) Pendry, J. B. *Science* **2004**, *306*, 1353–1355.
(5) Li, Z.; Mutlu, M.; Ozbay, E. *J. Opt.* **2013**, *15*, 023001.
(6) Gubler, U.; Bosshard, C. *Nat. Mater.* **2002**, *1*, 209–210.
(7) Zhao, R.; Zhou, J.; Koschny, T.; Economou, E. N.; Soukoulis, C. M. *Phys. Rev. Lett.* **2009**, *103*, 103602.
(8) Gansel, J. K.; Thiel, M.; Rill, M. S.; Decker, M.; Bade, K.; Saile, V.; Von Freymann, G.; Linden, S.; Wegener, M. *Science* **2009**, *325*, 1513–1515.
(9) Hodgkinson, I.; Wu, Q. H. *Adv. Mater.* **2001**, *13*, 889–897.
(10) Tang, Y.; Cohen, A. E. *Science* **2011**, *332*, 333–336.
(11) Hendry, E.; Carpy, T.; Johnston, J.; Popland, M.; Mikhaylovskiy, R. V.; Lapthorn, A. J.; Kelly, S. M.; Barron, L. D.; Gadegaard, N.; Kadodwala, M. *Nat. Nanotechnol.* **2010**, *5*, 783–787.

(12) Wu, X.; Xu, L.; Liu, L.; Ma, W.; Yin, H.; Kuang, H.; Wang, L.; Xu, C.; Kotov, N. A. *J. Am. Chem. Soc.* **2013**, *135*, 18629−18636.
(13) Dolamic, I.; Knoppe, S.; Dass, A.; Bürgi, T. *Nat. Commun.* **2012**, *3*, 1802.
(14) Gautier, C.; Bürgi, T. *Chem. Phys. Chem.* **2009**, *10*, 483−492.
(15) Yan, W.; Xu, L.; Xu, C.; Ma, W.; Kuang, H.; Wang, L.; Kotov, N. A. *J. Am. Chem. Soc.* **2012**, *134*, 15114−15121.
(16) Ma, W.; Kuang, H.; Wang, L.; Xu, L.; Chang, W.-S.; Zhang, H.; Sun, M.; Zhu, Y.; Zhao, Y.; Liu, L.; Xu, C.; Link, S.; Kotov, N. A. *Sci. Rep.* **2013**, *3*, 1934.
(17) Hentschel, M.; Schäferling, M.; Weiss, T.; Liu, N.; Giessen, H. *Nano Lett.* **2012**, *12*, 2542−2547.
(18) (a) Guerrero-Martínez, A.; Auguié, B.; Alonso-Gómez, J. L.; Džolič, Z.; Gómez-Graña, S.; Žinić, M.; Cid, M. M.; Liz-Marzán, L. M. *Angew. Chem., Int. Ed.* **2011**, *50*, 5499−5503. (b) George, J.; Thomas, G. *J. Am. Chem.Soc.* **2010**, *132*, 2502−2503. (c) Song, C.; et al. *Nano Lett.* **2013**, *13*, 3256−3261.
(19) Li, Y.; Liu, M. *Chem. Commun.* **2008**, 5571−5573.
(20) Xie, J.; Che, S. *Chem.—Eur. J.* **2012**, *18*, 15954−15959.
(21) Kuzyk, A.; Schreiber, R.; Fan, Z.; Pardatscher, G.; Roller, E. M.; Högele, A.; Simmel, F. C.; Govorov, A. O.; Liedl, T. *Nature* **2012**, *483*, 311−314.
(22) Leroux, F.; Gysemans, M.; Bals, S.; Batenburg, K. J.; Snauwaert, J.; Verbiest, T.; Van Haesendonck, C.; Van Tendeloo, G. *Adv. Mater.* **2010**, *22*, 2193−2197.
(23) Wang, R. Y.; Wang, H.; Wu, X.; Ji, Y.; Wang, P.; Qu, Y.; Chung, T. S. *Soft Matter* **2011**, *7*, 8370−8375.
(24) Zhu, Z.; Liu, W.; Li, Z.; Han, B.; Zhou, Y.; Gao, Y.; Tang, Z. *ACS Nano* **2012**, *6*, 2326−2332.
(25) Li, Z.; Zhu, Z.; Liu, W.; Zhou, Y.; Han, B.; Gao, Y.; Tang, Z. *J. Am. Chem. Soc.* **2012**, *134*, 3322−3325.
(26) Infusino, M.; De Luca, A.; Ciuchi, F.; Ionescu, A.; Scaramuzza, N.; Strangi, G. *Mol. Cryst. Liq. Cryst.* **2013**, *572*, 59−65.
(27) Ayeb, H.; Grand, J.; Sellame, H.; Truong, S.; Aubard, J.; Felidj, N.; Mlayah, A.; Lacaze, E. *J. Mater. Chem.* **2012**, *22*, 7856−7862.
(28) Qi, H.; Hegmann, T. *Liq. Cryst. Today* **2011**, *20*, 102−114.
(29) Zapotocky, M.; Ramos, L.; Poulin, P.; Lubensky, T. C.; Weitz, D. A. *Science* **1999**, *283*, 209−212.
(30) Liu, Q.; Senyuk, B.; Tang, J.; Lee, T.; Qian, J.; He, S.; Smalyukh, I. I. *Phys. Rev. Lett.* **2012**, *109*, 088301.
(31) Bitar, R.; Agez, G.; Mitov, M. *Soft Matter* **2011**, *7*, 8198−8206.
(32) Fan, Z.; Govorov, A. O. *Nano Lett.* **2010**, *10*, 2580−2587.
(33) Govorov, A. O.; Gun'Ko, Y. K.; Slocik, J. M.; Gérard, V. A.; Fan, Z.; Naik, R. R. *J. Mater. Chem.* **2011**, *21*, 16806−16818.
(34) Revol, J. F.; Bradford, H.; Giasson, J.; Marchessault, R. H.; Gray, D. G. *Int. J. Biol. Macromol.* **1992**, *14*, 170−172.
(35) Edgar, C. D.; Gray, D. G. *Cellulose* **2001**, *8*, 5−12.
(36) Dong, X. M.; Gray, D. G. *Langmuir* **1997**, *13*, 2404−2409.
(37) Habibi, Y.; Lucia, L. A.; Rojas, O. J. *Chem. Rev.* **2010**, *110*, 3479−3500.
(38) Moon, R. J.; Martini, A.; Nairn, J.; Simonsen, J.; Youngblood, J. *Chem. Soc. Rev.* **2011**, *40*, 3941−3994.
(39) Beck, S.; Bouchard, J.; Berry, R. *Biomacromolecules* **2011**, *12*, 167−172.
(40) Xue, M. D.; Kimura, T.; Revol, J. F.; Gray, D. G. *Langmuir* **1996**, *12*, 2076−2082.
(41) Shopsowitz, K. E.; Qi, H.; Hamad, W. Y.; MacLachlan, M. J. *Nature* **2010**, *468*, 422−426.
(42) Shopsowitz, K. E.; Hamad, W. Y.; MacLachlan, M. J. *Angew. Chem., Int. Ed.* **2011**, *50*, 10991−10995.
(43) Qi, H.; Shopsowitz, K. E.; Hamad, W. Y.; MacLachlan, M. J. *J. Am. Chem. Soc.* **2011**, *133*, 3728−3731.
(44) Kelly, J. A.; Shopsowitz, K. E.; Ahn, J. M.; Hamad, W. Y.; MacLachlan, M. J. *Langmuir* **2012**, *28*, 17256−17262.
(45) Nikoobakht, B.; El-Sayed, M. A. *Chem. Mater.* **2003**, *15*, 1957−1962.
(46) Khalil, O. S. *Clin. Chem.* **1999**, *45*, 165−177.
(47) De Vries, H. *Acta Crystallogr.* **1951**, *4*, 219−226.
(48) Woolley, J. T. *Plant Physiol.* **1975**, *55*, 172−174.
(49) Bos, A. *J. Appl. Polym. Sci.* **1972**, *16*, 2567−2576.
(50) Zhang, Y. P.; Chodavarapu, V. P.; Kirk, A. G.; Andrews, M. P. *J. Nanophoton.* **2012**, *6*, 063516.
(51) von Freymann, G.; Kitaev, V.; Lotsch, B. V.; Ozin, G. A. *Chem. Soc. Rev.* **2013**, *42*, 2528−2554.
(52) Majoinen, J.; Kontturi, E.; Ikkala, O.; Gray, D. G. *Cellulose* **2012**, *19*, 1599−1605.
(53) Mitov, M.; Dessaud, N. *Liq. Cryst.* **2007**, *34*, 183−193.
(54) Tschierske, C. *Angew. Chem., Int. Ed.* **2013**, *52*, 8828−8878.
(55) Link, S.; Mohamed, M. B.; El-Sayed, M. A. *J. Phys. Chem. B* **1999**, *103*, 3073−3077.